Research Article Vol. 3, No. 9 / 15 Sep 2024 / Optics Continuum 1722
OPTICS CONTINUUM

Optimized two-layer random motheye structures for SiO_2 windows

CHAORAN TU,[1] ZHIHAO HU,[2] JONATHAN HU,[2] CURTIS R. MENYUK,[1,*] THOMAS F. CARRUTHERS,[1] L. BRANDON SHAW,[3] LYNDA E. BUSSE,[3] AND JASBINDER S. SANGHERA[3]

[1]*Department of Computer Science and Electrical Engineering, University of Maryland Baltimore County, Baltimore, MD 21250, USA*
[2]*Department of Electrical and Computer Engineering, Baylor University, Waco, TX 76798, USA*
[3]*US Naval Research Lab, 4555 Overlook Ave SW, Washington, DC 20375, USA*
[*]*menyuk@umbc.edu*

Abstract: We computationally investigate the near-field transmission efficiency of two-layer motheye structures on SiO_2 windows. In these structures, a random motheye layer is imposed on top of a periodic motheye structure that consists of truncated pyramids. We first validate our simulation by comparing simulation results using a single layer of random pillars to experimental results. To maximize the transmission efficiency of our two-layer structures over the wavelength range of 0.4 to 2 μm, we used the previously optimized one-layer periodic pyramidal motheye structures as the bottom layer and we varied the statistical properties of the random pillars on the upper layer, which include the mean and span of their diameters and the mean and span of the pillar heights. We determine that the transmission generally increases as the range of the statistical parameters increases. It is theoretically possible to achieve an average transmission efficiency of 99.8% over the wavelength range from 0.4 to 2 μm by adding a random motheye layer over the periodic truncated pyramid structure, thereby increasing the average transmission efficiency by 0.3% over the same wavelength range and reducing the reflection by more than a factor of two. The large reduction in reflections over a broad bandwidth can be important in optical systems that rely on minimal reflections.

1. Introduction

Motheye structures are periodic, biomimetic sub-wavelength nanostructures that are inspired by the cornea of certain moth species that have naturally evolved to suppress the reflection of the incident light [1–5]. Although conventional multilayer antireflective (AR) coatings [6–9] can achieve a high transmission over a broad bandwidth by increasing the number of layers whose effective refractive index reduces the impedance mismatch between the air and an optical material such as a SiO_2 substrate, motheye structures can achieve a high transmission over a broadband wavelength range, which makes fabrication relatively simpler by using a single material [10]. Additionally, motheye structures are mechanically and thermally stable [11,12], and research also shows that polymer coatings can protect motheye structure from physical damages [13]. Both random and periodic motheye structures have a higher laser-induced damage threshold (LIDT) than do traditional AR-coated surfaces [14–17]. Therefore, they are useful in many applications, including automotive glass [18,19], laser systems [20–22], fiber optics [13], and photovoltaics [23–28].

One-layer periodic motheye structures have proved successful in many applications, but they are typically limited in bandwidth [29]. Bioinspired compound lenses [30–32] and our previous work [33] found that adding a second motheye layer can increase the bandwidth over which the transmission remains large and the reflection remains small. However, adding an extra motheye

#537298 https://doi.org/10.1364/OPTCON.537298
Journal © 2024 Received 22 Jul 2024; accepted 22 Aug 2024; published 11 Sep 2024

OPTICS CONTINUUM

layer that is periodic would require a large improvement in the resolution of today's fabrication systems. Recently, it has been found that random motheye structures can suppress reflections and enhance near-field light transmission [11,16]. In addition, it has been demonstrated that metal or metallic oxide nanopatterns on top of micropatterns can lower the reflection [34–38]. In this paper, we numerically study a two-layer motheye structure using a single dielectric material, in which a random motheye structure is on top of a periodic motheye structure, as shown in Fig. 1. The goal is to increase the transmission as well as to reduce the reflection. It is possible to fabricate these structures using current technology. In prior work [39], we computationally studied the impact of increasing the variation of the diameter and the height, where both are uniformly distributed about their means within a range of variation that we refer to as the span. In this paper, we extend our prior work and investigate the near-field transmission efficiency of double-layer motheye structures that are fabricated on SiO_2 windows. The structure consists of a random motheye layer that is imposed on top of a periodic motheye layer that consists of truncated pyramids. We varied the mean and span of both the height and diameter of the random pillars in order to maximize the transmission in the wavelength range from 0.4 to 2 μm.

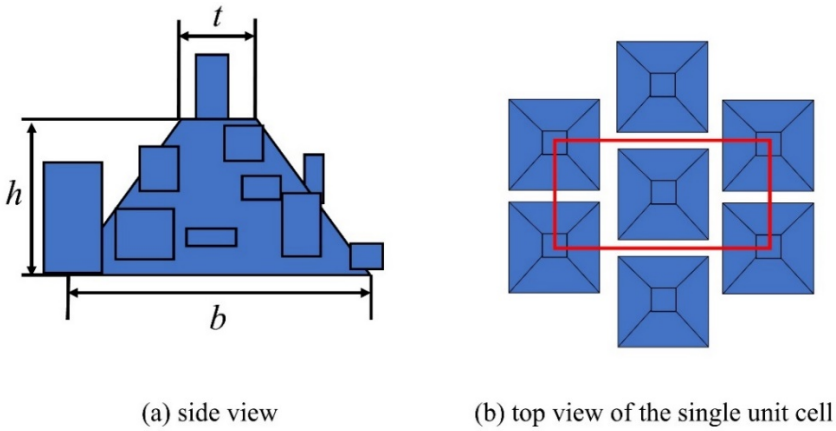

Fig. 1. Schematic diagram of the pyramid of the two-layer random motheye structure. (a) Side view of one pyramid with random pillars. (b) Top view of the single unit cell. The red box indicates the computational window. To better illustrate the pyramid structure, random pillars are excluded here.

In a one-layer structure, increasing the height of the motheye structures can lead to a higher transmission. However, there is a limit to the height of the motheye structure beyond which the transmission does not further increase [40,41]. Having another random layer on top of the periodic layer will lead to an enhanced transmission over a broader bandwidth. In addition, the diffraction limit is proportional to the pitch of the periodic pattern [38,42,43]. Making the structure size smaller would be a direct solution to avoid the diffraction limit. However, it is not currently possible to fabricate regular structures with the small feature size of a random layer. In this paper, we only study the near-field transmission before the signal has a chance to diffract.

The remainder of this paper is organized as follows: In Sec. 2, we validate our simulation for single layer random motheye structures by comparing our simulation results to experimental results. In Sec. 3, we introduce our two-layer random motheye structure in which a random motheye layer is imposed on a periodic truncated pyramid motheye layer, both of which can be fabricated [44]. In Sec. 4, we report our optimization results, and compare the transmission performance of the two-layer random motheye layers to the transmission performances of the one-layer periodic and one-layer random motheye structures. To verify that our computational

OPTICS CONTINUUM

window is sufficiently large, we quadrupled our computational window to include four unit cells, and we show the converged transmission spectrum in Sec. 5. Finally, we conclude in Sec. 6.

2. Comparison with experimental results using one-layer random motheye structure

Our model was first validated by comparing our simulation results to experimental results using a one-layer random motheye structure. We used the open-source finite-difference time-domain (FDTD) software package MEEP that is available under the GNU General Public License [45]. We use a spatial resolution of 5 nm for all simulations in this section. We simulated a portion of a random motheye structure that has a cross-sectional area of $0.75\,\mu\text{m} \times 0.75\,\mu\text{m}$, as shown in a top view in Fig. 2(a), and we use periodic boundary conditions. In our study, any light that is scattered from the structure is included in the reflection. The red box in Fig. 1(b) indicates the computational window in our simulation. We found that further increasing the computational window does not significantly change simulation results. It is also sufficient to study a single polarization of the incoming light, since the results do not depend on the light's polarization in random structures, which is the case for most applications [4,46]. The effect of non-normal incidence has been discussed for example in [4]. We used a broadband plane wave source that is located on top of random pillars. The glass dispersion in refractive index is also included in the simulation [47]. We calculated transmission and reflection spectra by taking a Fourier transform of the time-domain flux through surfaces lying just below and above the motheye structure. Consistent with the experimental scanning electron micrograph (SEM) data from Fig. 6 in Ref. [11], we used a uniform random distribution for the diameter that varies between $0.10–0.01 = 0.09\,\mu$m and $0.10 + 0.01 = 0.11\,\mu$m, so that the mean is $0.1\,\mu$m and the span is $0.02\,\mu$m [11]. We also used a uniform random distribution for the height that varies over the range $0.617 \pm 0.03\,\mu$m, so that its mean is $0.617\,\mu$m and its span is $0.06\,\mu$m. Consistent with the SEM data, we used 25 pillars that are randomly positioned in our computational window. If we found that any of the pillars runs into another pillar or a boundary, we generate a new pillar location until all pillars are inside the computational window without running into each other. Figure 2(b) compares our simulation results to the experimental results, which were extracted from Fig. 7 in Ref. [11]. We ran 10 realizations of different random structures, and we show the average reflection in Fig. 2(b) [39]. We also verified that increasing the number of realizations to 20 will

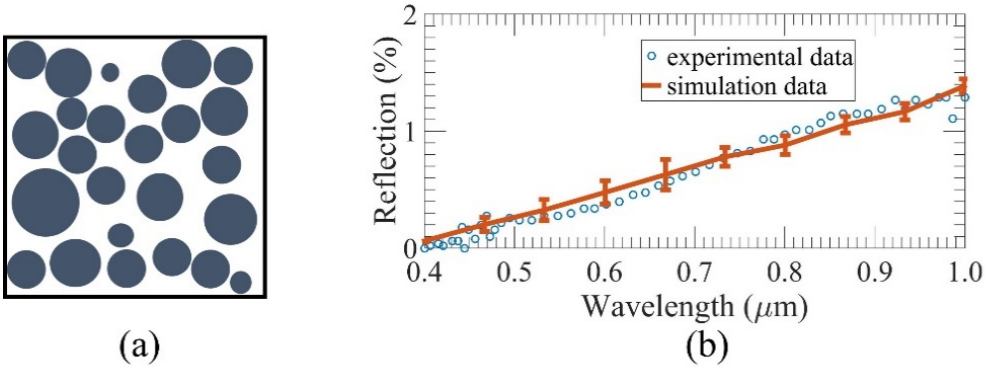

Fig. 2. (a) Top view of a random structure. (b) Simulation and experimental reflection spectra on random motheye structures. We use a uniform random distribution for the diameter with parameters of $0.10 \pm 0.01\,\mu$m (a span of $0.02\,\mu$m) and a uniform random distribution for the height of the pillars with parameters of $0.617 \pm 0.030\,\mu$m (a span of $0.06\,\mu$m). The experimental results are extracted from Fig. 7 in Ref. [11].

OPTICS CONTINUUM

not change the transmission, so that 10 realizations is sufficient. The error bars represent the standard deviation. The simulations are in very good agreement with the experiments, in which it was found that the reflection is less than 0.1% at a wavelength of 0.4 μm and less than 2% between 0.4 μm and 1.0 μm.

3. Modeling the random layer on top of the periodic pyramid layer

We next considered a two-layer structure where random pillars are placed on top of the periodic truncated pyramids, shown schematically in Fig. 1(a). For the bottom layer, we used a structure of truncated periods that we previously optimized to maximize the average transmission in the wavelength range of 0.4 to 2.0 μm and that can be fabricated [41,48]. For the top layer, we used a structure of random pillars that can also be fabricated [11,16]. For the bottom layer in which we used periodic truncated pyramids, we chose a top width $t = 0.15$ μm, a bottom width $b = 0.95$ μm, and a height $h = 0.6$ μm, consistent with our previous optimization study [41]. Due to the small dimension of the upper random pillars, we used a minimum spatial resolution of 1 nm in our simulations. Further decreasing spatial resolution did not significantly change the simulation results. We averaged the transmission spectra from 10 realizations, and we verified that the results have converged by comparing to results using 20 realizations. We thereby simulate the behavior that is expected in an experiment that effectively averages over many unit cells. Figure 1(b) shows the top view of the computational window of the two-layer random motheye structures, simplified by excluding the random structures and highlighting the spacing of the truncated pyramids. The computational window has a dimension of $S_x = 1.0$ μm and $S_y = \sqrt{3}S_x = 1.732$ μm. The pitch of the bottom layer is selected based on experiments [16]. The height of the entire computational window is 8 μm, and the perfectly matched layer (PML) [45] has a thickness d_{PML} of 1 μm at the top and the bottom of the computational window. We use a spatial resolution of 5 nm. Each simulation will stop when the remaining field has a factor of 10^8 less than the input field. The output transmission spectrum has a resolution of 0.05 μm.

We studied the variation of the transmission as we varied each of the four parameters, the mean diameter d_m, the span of the diameter d_s, the mean height h_m, and the span of the height h_s, keeping the other three fixed. The starting point of the study was the structure with $d_m = 0.15$ μm, $d_s = 0.08$ μm, $h_m = 0.5$ μm, and $h_s = 0.8$ μm. We varied the mean diameter d_m from 0.05 to 0.15 μm; we varied the mean height h_m from 0.1 to 0.5 μm; we varied the span of the diameter d_s from 0 to 0.04 μm; and, finally, we varied the span of the height h_s from 0 to 0.4 μm. We show the results in Fig. 3. A maximum of complete 100% transmission is achieved at the starting point of our study when the wavelength equals 0.98 μm. Over the wavelength range that we considered, 0.4 to 2 μm, the average transmission increased by at least 0.002 when we varied d_m and h_m and by 0.001 when we varied d_s and h_s.

In addition to individual studies in which we varied the spans and the means of the pillar heights and diameters we studied transmission when the spans and means change together. In Fig. 4, we show the average transmission when varying the diameter mean d_m and span d_s while the height mean h_m and span h_s are fixed at 0.5 μm and 0.4 μm, respectively. We demonstrate that a larger mean diameter and a larger diameter span will lead to a higher transmission, for the parameters that we consider to be consistent with the experimental results [11].

In Fig. 5, we show the average transmission when varying height mean h_m and span h_s while the diameter mean d_m and span d_s are fixed at 0.15 μm and 0.1 μm, respectively. We do not plot results when h_s is larger than h_m since these values are unphysical. We find that we can achieve a higher average transmission with larger mean height and height span.

OPTICS CONTINUUM

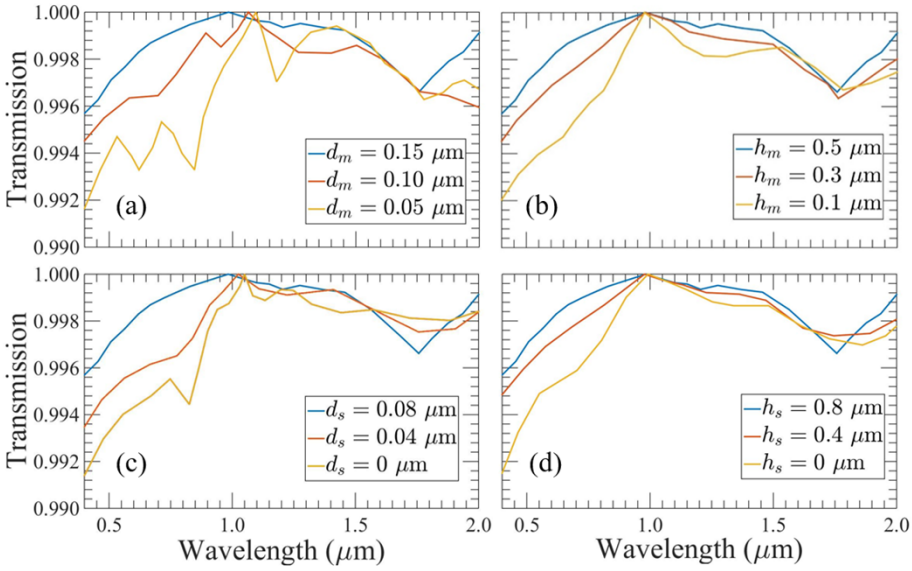

Fig. 3. (a) Transmission spectra when varying the mean diameter of the random pillars with fixed $h_m = 0.5$ μm, $d_s = 0.08$ μm, and $h_s = 0.8$ μm. (b) Transmission spectra when varying the mean height of the random pillars with fixed $d_m = 0.15$ μm, $d_s = 0.08$ μm, and $h_s = 0.8$ μm. (c) Transmission spectra when varying the diameter span of the random pillars with fixed $d_m = 0.15$ μm, $h_m = 0.5$ μm, and $h_s = 0.8$ μm. (d) Transmission spectra when varying the height span of the random pillars with fixed $d_m = 0.15$ μm, $h_m = 0.5$ μm, and $d_s = 0.08$ μm. The parameters d_m, d_s, h_m, and h_s represent diameter mean, diameter span, height mean, and height span, respectively.

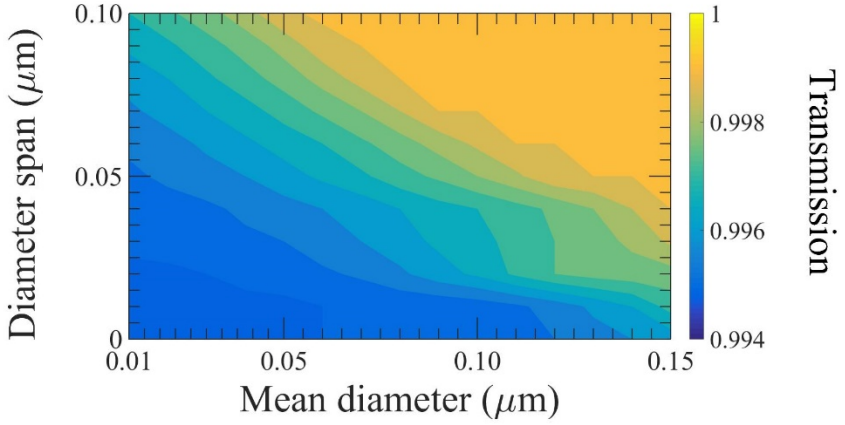

Fig. 4. Average transmission when varying diameter mean d_m and diameter span d_s of the upper random pillars with fixed $h_m = 0.5$ μm and $h_s = 0.2$ μm.

OPTICS CONTINUUM

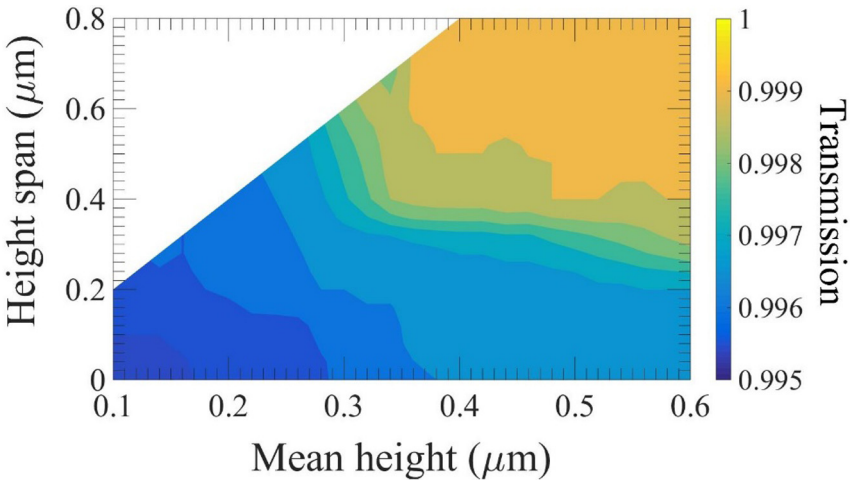

Fig. 5. Average transmission when varying the height mean h_{m} and height span h_{s} of the upper random pillars with fixed $d_m = 0.15\ \mu$m and $d_s = 0.02\ \mu$m.

4. Comparison of the optimal spectra

We now compare the results of the two-layer random motheye structure with the optimized results of the one-layer periodic motheye structures and the one-layer random motheye structure in Fig. 6.

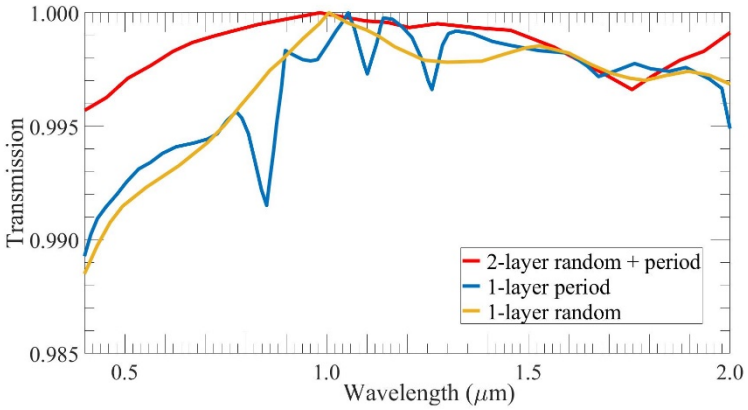

Fig. 6. Averaged transmission spectra of (blue) a random motheye structure layer ($d_m = 0.15\,\mu$m, $d_s = 0.08\,\mu$m, $h_m = 0.5\,\mu$m, and $h_s = 0.8\,\mu$m) imposed onto a periodic motheye structure layer ($t = 0.15\,\mu$m, $b = 0.95\,\mu$m, $h = 0.6\,\mu$m) of 10 realizations; (red) a one-layer periodic truncated motheye structure ($t = 0.15\,\mu$m, $b = 0.95\,\mu$m, $h = 0.6\,\mu$m); (orange) a one-layer random motheye structure ($d_m = 0.15\,\mu$m, $d_s = 0.08\,\mu$m, $h_m = 0.5\,\mu$m, and $h_s = 0.8\,\mu$m of 10 realizations.

Based on the transmission spectra from the previous section, we chose a two-layer random motheye structure whose upper layer consists of random pillars with a mean diameter of 0.15 μm, a mean height of 0.5 μm, a diameter span of 0.04 μm, and a height span of 0.4 μm. The lower layer consists of periodic truncated pyramids with a top width of 0.15 μm, a bottom width of 0.95 μm, and a height of 0.6 μm. The two-layer structure yields an average transmission of 99.8% over a wavelength range of 0.4 μm to 2.0 μm. We also show the transmission spectrum for a one-layer periodic SiO_2 motheye structure that has the same dimensions as the bottom layer pyramids of

OPTICS CONTINUUM

the two-layer random motheye structure; this structure has an average transmission of 99.5% from 0.4 μm to 2.0 μm. In addition, we show the transmission spectrum of a one-layer random motheye structure that possesses the same parameters as the random top layer in the two-layer random structure; the average transmission here is 99.5% from 0.4 to 2.0 μm. We expect that larger variations in the upper random layer will lead to an even higher transmission. However, we used the same random variations in the one- and two-layer structure to have a fair comparison. We note that these parameters are experimentally achievable [8]. Hence, we conclude that the two-layer random motheye can achieve a better transmission than the optimal one-layer motheye structure. Sharp dips in the transmission of the one-layer periodic structure that we attribute to resonances are effectively smoothed over and disappear when a random layer with a sufficiently high mean diameter and height with sufficient spans are used.

The transmission difference between 99.5% and 99.8% for the one- and two-layer random structures may appear small. However, the reflection is reduced from 0.5% to 0.2%, which is a large difference and can be important for some applications, such as increasing the damage threshold for high-power fiber lasers [49].

5. Verification of randomness

In order to validate that our computational window is sufficiently large to simulate the average over many unit cells that is expected in an experiment, we have carried out simulations in which we quadrupled the size of the computational window. Figure 7 shows the computational window marked with a green dashed line that is four times larger than the previous computational window marked by red solid line and now includes four unit cells.

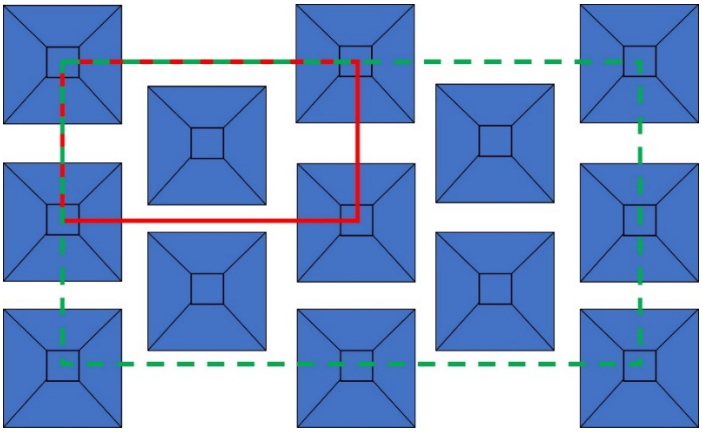

Fig. 7. The computational window marked with green dash lines that is now four times larger than the previous computational window marked by red solid lines.

The transmission spectra of the quadrupled computational window and the original computation window are shown in Fig. 8. In both simulations, we averaged the transmission spectrum over 10 realizations. The results for the two computational windows agree, implying that it is sufficient to use a computational window that consists of one unit cell.

OPTICS CONTINUUM

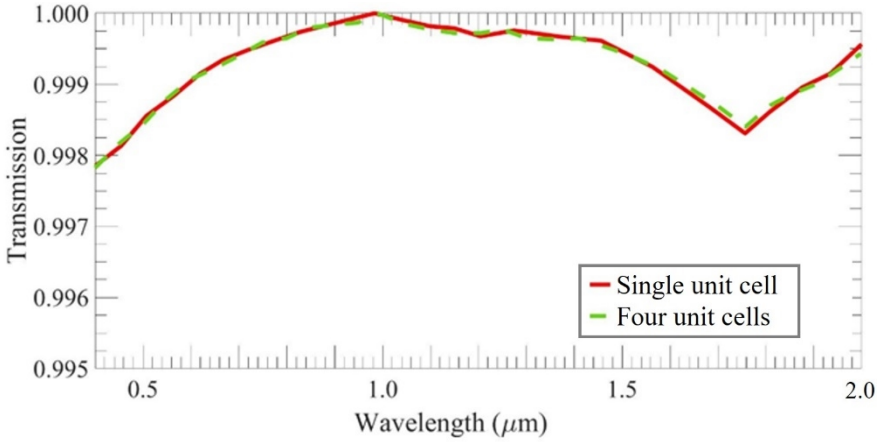

Fig. 8. The transmission spectra of random motheye structures using a computational window of single unit cell (red solid line) and quadrupled computational window of four unit cells (green dashed line).

6. Conclusion

We used the FDTD method to computationally study the near-field transmission of light that is normally incident on a SiO_2 glass window with a two-layer motheye structure, where a layer of random pillars is added on top of a periodic layer of truncated pyramids. We investigated the effect of changing the mean diameter, the mean height, the diameter span, and the height span of the random pillars. We found that the transmission generally increases as the randomness increases, which is the case when the random pillars have a large mean diameter, a large mean height, and both have large spans. The optimal two-layer random motheye structure has an overall transmission that is above 99.5%, and the average transmission is 99.8% from 0.4 to 2 μm. The reduction in the average reflection from a single-layer random motheye structure is more than a factor of two.

Funding. U.S. Naval Research Laboratory (N00173-15-1-G905).

Acknowledgement. A portion of our computational work was carried out at UMBC High Performance Computing Facility.

Disclosures. The authors declare no conflicts of interest.

Data availability. Data underlying the results presented in this paper are not publicly available at this time but may be obtained from the authors upon reasonable request.

References

1. Y. Ou, D. Corell, C. Dam-Hansen, *et al.*, "Antireflective sub-wavelength structures for improvement of the extraction efficiency and color rendering index of monolithic white light-emitting diode," Opt. Express **19**(S2), A166–A172 (2011).
2. C. G. Bernhard and W. H. Miller, "A corneal nipple pattern in insect compound eyes," Acta Physiol. Scand. **56**(3-4), 385–386 (1962).
3. R. Brunner, O. Sandfuchs, C. Pacholski, *et al.*, "Lessons from nature: biomimetic subwavelength structures for high-performance optics," Laser Photonics Rev. **5**, 1–19 (2011).
4. Y.-F. Huang, S. Chattopadhyay, Y.-J. Jen, *et al.*, "Improved broadband and quasi-omnidirectional anti-reflection properties with biomimetic silicon nanostructures," Nat. Nanotechnol. **2**(12), 770–774 (2007).
5. D. G. Stavenga, S. Foletti, G. Palasantzas, *et al.*, "Light on the moth-eye corneal nipple array of butterflies," Proc. R. Soc. London, Ser. B **273**(1587), 661–667 (2006).
6. K.V. Popov, J. A. Dobrowolski, A. V. Tikhonravov, *et al.*, "Broadband high-reflection multilayer coatings at oblique angles of incidence," Appl. Opt. **36**(10), 2139–2151 (1997).
7. J. D. Wheeler, B. Koopman, P. Gallardo, *et al.*, "Antireflection coatings for submillimeter silicon lenses," Proc. SPIE **9153**, 91532Z (2014).

OPTICS CONTINUUM

8. F. Defrance, C. Jung-Kubiak, J. Sayers, *et al.*, "1.6:1 bandwidth two-layer antireflection structure for silicon matched to the 190–310 GHz atmospheric window," Appl. Opt. **57**(18), 5196–5209 (2018).
9. T. Macioce, F. Defrance, C. Jung-Kubiak, *et al.*, "Multilayer etched antireflective structures for silicon vacuum windows," J. Low Temp. Phys. **199**(3-4), 935–942 (2020).
10. L. Busse, C. Florea, L. B. Shaw, *et al.*, "Anti-reflective surface structures for high energy laser applications," in *Annual Directed Energy Symposium* (2013), paper 13-Symp-053.
11. D. S. Hobbs, B. D. MacLeod, and J. R. Riccobono, "Update on the development of high-performance anti-reflecting surface relief micro-structures," Proc. SPIE **6545**, 65450Y (2007).
12. J. Sanghera, C. Florea, L. Busse, *et al.*, "Reduced Fresnel losses in chalcogenide fibers by using anti-reflective surface structures on fiber end faces," Opt. Express **18**(25), 26760–26768 (2010).
13. X. Yu, K. Goto, Y. Yasunaga, *et al.*, "Polymer-coated moth-eye hybrid structure for broadband antireflection in the terahertz region," Opt. Lett. **46**(15), 3761–3764 (2021).
14. D. S. Hobbs, B. D. MacLeod, E. Sabatino, *et al.*, "Laser damage resistant antireflection microstructures in Raytheon ceramic YAG, sapphire, ALON, and quartz," Proc. SPIE **8016**, 80160 T (2011).
15. C. Florea, L. Busse, S. Bayyab, *et al.*, "Anti-reflective surface structures in spinel ceramic windows," in the *10th Pacific Rim Conference on Ceramic and Glass Technology* (2013), paper S10-014.
16. L. E. Busse, C. M. Florea, J. A. Frantz, *et al.*, "Anti-reflective surface structures for spinel ceramics and fused silica windows, lenses, and optical fibers," Opt. Mater. Exp. **4**(12), 2504–2515 (2014).
17. Z. Teng, Y. Sun, F. Kong, *et al.*, "Sub-wavelength microstructures on lithium triborate surface with high transmittance and laser-induced damage threshold at 1064 nm," Opt. Laser Technol. **145**, 107487 (2022).
18. Y. M. Song, Y. Jeong, C. Yeo, *et al.*, "Enhanced power generation in concentrated photovoltaics using broadband antireflective cover glasses with moth eye structures," Opt. Express **20**(S6), A916–A923 (2012).
19. J. Kulakofsky, W. Lewis, M. Robertson, *et al.*, "Designing high-power components for optical telecommunications," Proc. SPIE **4679**, 198 (2002).
20. R. J. Weiblen, C. R. Menyuk, L. E. Busse, *et al.*, "Optimized moth-eye anti-reflective structures for As2S3 chalcogenide optical fibers," Opt. Express **24**(10), 10172–10187 (2016).
21. X. Yu, Y. Yasunaga, K. Goto, *et al.*, "Profile control of femtosecond laser-fabricated moth-eye structures on Si substrate," Opt. Lasers Eng. **142**, 106584 (2021).
22. R. Contractor, G. D'Aguanno, and C. R. Menyuk, "Ultra-broadband, polarization-independent, wide-angle absorption in impedance-matched metamaterials with anti-reflective moth-eye surfaces," Opt. Express **26**(18), 24031–24043 (2018).
23. S. A. Boden and D. M. Bagnall, "Optimization of moth-eye antireflection schemes for silicon solar cells," Prog. Photovolt: Res. Appl. **18**(3), 195–203 (2010).
24. J. Oh, H. C. Yuan, and H. M. Branz, "An 18:2%-efficient black-silicon solar cell achieved through control of carrier recombination in nanostructures," Nat. Nanotechnol. **7**(11), 743–748 (2012).
25. G. Cossio, E. D. Yu, S. R. Tatavarti, *et al.*, "Omnidirectional current enhancement from laminated moth-eye textured polymer packaging for large-area, flexible III-V Solar Modules," IEEE Journal of Photovoltaics **11**(3), 685–691 (2021).
26. D. Du, Z. Xu, L. Wang, *et al.*, "The broadband and omnidirectional antireflective performance of perovskite solar cells with curved nanostructures," Sol. Energy **224**, 10–17 (2021).
27. S. Ju, M. Byun, M. Kim, *et al.*, "Fabrication of perovskite solar cell with high short-circuit current density (Jsc) using moth-eye structure of SiO_x," Nano Res. **13**(4), 1156–1161 (2020).
28. K. Peng, Y. Xu, Y. Wu, *et al.*, "Aligned single-crystalline Si nanowire arrays for photovoltaic applications," Small **1**(11), 1062–1067 (2005).
29. Z. Han, Z. Jiao, S. Niu, *et al.*, "Ascendant bioinspired antireflective materials: Opportunities and challenges coexist," Prog. Mater. Sci. **103**, 1–68 (2019).
30. F. Chiadini, V. Fiumara, A. Scaglione, *et al.*, "Simulation and analysis of prismatic bioinspired compound lenses for solar cells," Bioins. Biomim **5**(2), 1748–3182 (2010).
31. F. Chiadini, V. Fiumara, A. Scaglione, *et al.*, "Simulation and analysis of prismatic bioinspired compound lenses for solar cells: II. Multifrequency analysis," Bioins. Biomim **6**(1), 1748–3182 (2010).
32. D. P. Pulsifer, A. Lakhtakia, R.J. Martin-Palma, *et al.*, "Engineered biomimicry: polymeric replication of surface features found on insects," Proc. SPIE **7975**, 79750O (2011).
33. C. Tu, J. Hu, C. R. Menyuk, *et al.*, "Optimized two-layer motheye structures for $MgAl_2O_4$ spinel ceramic windows," OSA Continuum **4**(8), 2143–2153 (2021).
34. B. Dudem, L. K. Bharat, J. W. Leem, *et al.*, "Hierarchical Ag/TiO_2/Si forest-like nano/micro-architectures as antireflective, plasmonic photocatalytic, and self-cleaning coatings," ACS Sustainable Chem. Eng. **6**(2), 1580–1591 (2018).
35. J. W. Leem, B. Dudem, and J. S. Yu, "Biomimetic nano/micro double-textured silicon with outstanding antireflective and super-hydrophilic surfaces for high optical performance," RSC Adv. **7**(54), 33757–33763 (2017).
36. S. H. Kim, S. H. Lee, B. Dudem, *et al.*, "Fabrication and optical characterization of hybrid antireflective structures with zinc oxide nanorods/micro pyramidal silicon for photovoltaic applications," Opt. Mater. Express **6**(12), 4000–4009 (2016).

OPTICS CONTINUUM

37. J. Cai and L. Qi, "Recent advances in antireflective surfaces based on nanostructure arrays," Mater. Horiz. **2**(1), 37–53 (2015).
38. J. W. Leem, Y. M. Song, and J. S. Yu, "Biomimetic artificial Si compound eye surface structures with broadband and wide-angle antireflection properties for Si-based optoelectronic applications," Nanoscale **5**(21), 10455–10460 (2013).
39. C. Tu, J. Hu, C. R. Menyuk, *et al.*, "Optimization of random motheye structures for silica windows with normally incident light," in *OSA Advanced Photonics Congress* 2021, paper NoF2C.6.
40. S. Ji, K. Song, T. B. Nguyen, *et al.*, "Optimal moth eye nanostructure array on transparent glass towards broadband antireflection," ACS Appl. Mater. Interfaces **5**(21), 10731–10737 (2013).
41. C. Tu, J. Hu, C. R. Menyuk, *et al.*, "Optimal dimensions of cone and pyramid motheye structures for SiO2 silica windows," arXiv, (2023).
42. S. J. Wilson and M. C. Hutley, "The optical properties of 'Moth Eye' antireflection surfaces," Optica Acta: International Journal of Optics **29**(7), 993–1009 (1982).
43. C. Brückner, T. Käsebier, B. Pradarutti, *et al.*, "Broadband antireflective structures applied to high resistive float zone silicon in the THz spectral range," Opt. Express **17**(5), 3063–3077 (2009).
44. C. Tu, C. R. Menyuk, L. B. Shaw, *et al.*, "Optimized cone-shaped motheye structures for fused silica glass windows," in *Frontiers in Optics / Laser Science*, paper JW6A.11 (2020).
45. A. F. Oskooi, D. Roundy, M. Ibanescu, *et al.*, "MEEP: A flexible free-software package for electromagnetic simulations by the FDTD method," Comp. Phys. Comm. **181**(3), 687–702 (2010).
46. M. Steel, T. White, C. M. de Sterke, *et al.*, "Symmetry and degeneracy in microstructured optical fibers," Opt. Lett. **26**(8), 488–490 (2001).
47. I. H. Malitson, "Interspecimen Comparison of the Refractive Index of Fused Silica," J. Opt. Soc. Am. **55**(10), 1205–1209 (1965).
48. R. J. Weiblen, C. Florea, L. Busse, *et al.*, "Irradiance enhancement and increased laser damage threshold in As2S3 moth-eye antireflective structures," Opt. Lett. **40**, 4799–4802 (2015).
49. J. Nilsson and D. N. Payne, "High-power fiber lasers," Science **332**(6032), 921–922 (2011).